Design of a CT Saturation Detection Technique with the Countermeasure for a Spike Signal

Yong-Cheol Kang* and Jae-Sung Yun*

Abstract-When a current transformer (CT) is saturated, the wave-shape of the secondary current is distorted and contains points of inflection, which correspond to the start or end of each saturation period. Discontinuity in the first-difference function of the current arises at points of inflection, where the second and third differences convert into pulses that can be used to detect saturation. This paper describes the design and evaluation of a CT saturation detection technique using the third-difference function and includes the countermeasure for a spike signal. Test results clearly demonstrate that the algorithm successfully detects the start and end of each saturation period irrespective of the remanent flux and magnetization inductance in the saturated region. This paper concludes by describing the results of hardware implementation of the algorithm using a DSP.

Keywords: Remanent flux, Spike signal, Third-difference, Point of inflection

1. Introduction

Current transformer (CT) saturation distorts the wave-shape of the secondary current signals. The distortion may cause operation malfunctions of a protection relay. To minimize the effect, protection relays are normally designed to cope with saturation by using large CTs in conjunction with relaying algorithms insensitive to the effects of saturation.

Phadke and Thorp suggested a method for detecting the onset of CT saturation [1]. Their method relies on the abrupt change in the current when the CT enters saturation. Difficulties may arise if the current does not collapse to zero.

Kang et al. suggested an algorithm for calculating the core flux using the secondary current [2]. The flux is used to calculate the exciting current, which is then used to compensate the distorted current. However, this algorithm is based on the assumption that the remanent flux was zero when the fault occurred.

Fernandez proposed an impedance-based CT saturation detection algorithm for bus-bar differential protection [3]. This algorithm is based on the first order differential equation for the power system source impedance at the relay position and uses the voltage of the bus bar as well as current signal to detect CT saturation.

Kang et al. also proposed an algorithm for detecting CT saturation [4] that detects the start and end of each saturation period irrespective of the level of the remanent flux. Our paper describes the extensive study of the algorithm proposed by Kang et al. [4] and the theoretical background of determining the threshold value for saturation detection. We include the countermeasure for a spike, which can result from A/D conversion and the test results when the secondary time constant is very small. The algorithm was implemented on a prototype system based on a digital signal processor (DSP).

* Division of Electronics and Information Engineering, Chonbuk National Univ., NPTC Kang (yckang@moak.chonbuk.ac.kr, hana42@netian.com)

Received February 7, 2003 ; Accepted May 14, 2003

2. A CT Saturation Detection Algorithm

Fig. 1 shows a simplified equivalent circuit of a CT. When a fault occurs, the primary current satisfies (1).

$$i_1(t)=\begin{cases} I_{\max}[\cos(\omega t-\theta)-e^{-t/T_P}\cos\theta], & for\ t\geq 0 \\ 0, & for\ t<0 \end{cases} \quad (1)$$

where I_{max}, T_p, and θ are the maximum fault current, primary time constant, and fault inception angle.

The secondary current of a CT can be expressed as

$$i_2(t)=Ae^{-t/T_s}+Be^{-t/T_p}-C\sin(\omega t-\theta-\varphi) \quad (2)$$

where T_s is the secondary time constant and $\tan\varphi=\omega T_s$ [5]

The first and second terms in (2) decay with a time constant of T_p and T_s, respectively, and the magnitude of the sinusoid is

$$C=I_{\max}\omega T_s\cos\varphi=I_{\max}\sin\varphi=I_{\max}\frac{\omega T_s}{\sqrt{1+(\omega T_s)^2}}. \quad (3)$$

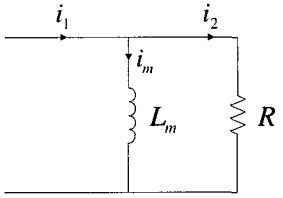

Fig. 1 Simplified equivalent circuit of a CT

The discrete-time version of $i_2(t)$ can be obtained by assuming $t = nT$, i.e.,

$$i_2[n] = Ae^{-nT/T_s} + Be^{-nT/T_p} - C\sin(\frac{2\pi}{N}n - \theta - \varphi) \quad (4)$$

where T is the sampling interval and N is the number of samples per cycle.

The first difference of $i_2[n]$ is

$$\begin{aligned} del1[n] &= i_2[n] - i_2[n-1] \\ &= A(1-e^{T/T_s})e^{-nT/T_s} + B(1-e^{T/T_p})e^{-nT/T_p} \cdot \\ &\quad - C(2\sin\frac{\pi}{N})\sin(\frac{2\pi}{N}n - \theta - \varphi - \frac{\pi}{N} + \frac{\pi}{2}) \end{aligned} \quad (5)$$

If the power system frequency is 60 Hz and $N = 64$, $T = 0.26$ ms. If $T_s = 1$ s and $T_p = 0.02$ s, the reduction rates of $(1 - e^{T/T_s})$ and $(1 - e^{T/T_p})$ for exponential terms will be 0.00026 and 0.0131, respectively, i.e., the exponential terms in $del1[n]$ are reduced to a negligible value.

If the magnitude of the sinusoid in $del1[n]$ is reduced to $2\sin(\pi/N)C = 0.098C$, i.e., a decrease of about 90%, then the reduction rate depends on N. Consequently, if $i_2[n]$ has the form of (4) and the time constants are sufficiently large, then the only component in $del1[n]$ is a sinusoid and its magnitude is $0.098C$.

The second and third differences of $i_2[n]$ are defined by

$$del2[n] = del1[n] - del1[n-1] \quad (6)$$

$$del3[n] = del2[n] - del2[n-1] \quad (7)$$

where $del2[n]$ and $del3[n]$ are sinusoids with magnitudes at $N = 64$ of $[2\sin(\pi/N)]^2C = 0.009604C$ and $[2\sin(\pi/N)]^3C = 0.000941C$, respectively. Hence, the magnitude of the sinusoid in $del3[n]$ is reduced to 0.1% of its value in $i_2[n]$.

If saturation starts at $n = m+1$ and ends at $n = k+1$ (where $k > m$), then m and k are two points of inflection. If $i_{21}[n]$, $i_{22}[n]$, and $i_{23}[n]$ are used to refer to the secondary currents before, during, and after saturation, then $i_{21}[n]$ and $i_{23}[n]$ have a waveform similar to (4) and $i_{22}[n]$ is either similar to (4) or similar to an exponential that collapses to zero when the CT saturates. The former case is discussed in Sections 2.1 to 2.4 and the latter in Section 2.5. In either case, each of the three signals is continuous and retains its form within its period. Hence, $i_{21}[m] = i_{22}[m]$ and $i_{22}[k] = i_{23}[k]$, but $i_{21}[m+1] \neq i_{22}[m+1]$ and $i_{22}[k+1] \neq i_{23}[k+1]$; note that $i_{21}[m+1]$ and $i_{22}[k+1]$ are virtual samples on the extended line rather than actual samples.

2.1 Features of *del1*[*n*]

Since $i_2[n]$ has the same form as (4), the exponential terms in $del1[n]$ can be ignored. Consequently, $del1[n]$ consists of sinusoids with different magnitudes in the saturated and unsaturated states. A discontinuity in $del1[n]$ arises at $m+1$ and $k+1$, which corresponds to the start or end of saturation.

2.2 Features of *del2*[*n*]

If $[2\sin(\pi/N)]^2C$ is very small, $del2[n]$ can be used as a detector. For example, if $C = 100$ A and $N = 64$, then $[2\sin(\pi/N)]^2C = 0.96$ A. Hence, $del2[n]$ in the interval $n \leq m$, $del2[n]$ is a sinusoid and its magnitude does not exceed 0.96 A. At $n = m+1$ (saturation start),

$$\begin{aligned} del2[m+1] &= i_{22}[m+1] - 2i_{22}[m] + i_{21}[m-1] \\ &= i_{22}[m+1] - 2i_{21}[m] + i_{21}[m-1] \end{aligned} \quad (8)$$

The approximation of (9) can be made with a maximum error of 0.96 A.

$$i_{21}[m+1] - 2i_{21}[m] + i_{21}[m-1] \approx 0 \quad (9)$$

$del2[m+1]$ can be approximated as $i_{22}[m+1] - i_{21}[m+1]$. As mentioned earlier, $i_{21}[m+1]$ is a virtual sample on the extended line and can be considered as the value at $n = m+1$ if the CT had not saturated. Thus, $del2[m+1]$ is larger than the current value of the saturation point. During the period $m+2 \leq n \leq k$ (saturated period), the magnitude of $del2[n]$, which is also a sinusoid, is smaller than before saturation.

At $n = k+1$ (saturation end),

$$\begin{aligned} del2[k+1] &= i_{23}[k+1] - 2i_{23}[k] + i_{22}[k-1] \\ &= i_{23}[k+1] - 2i_{22}[k] + i_{22}[k-1] \end{aligned} \quad (10)$$

Similarly, $del2[k+1] \approx i_{23}[k+1] - i_{22}[k+1]$ where $i_{22}[k+1]$ is a virtual sample on the extended line. The error is less than 0.96 and $del2[k+1]$ has a large value. In the interval of $k+2 \leq n$, $del2[n]$ is also a sinusoid.

Consequently, if $i_2[n]$ can be expressed in the form of (4), the magnitudes of $del2[n]$, which are sinusoids, are smaller than $[2\sin(\pi/N)]^2C$ except for the saturation start and ends. Therefore, $del2[n]$ can be used as a detector if $del2[m+1]$

and $del2[k+1]$ are much larger than $[2\sin(\pi/N)]^2C$.

2.3 Features of *del3[n]*

If $[2\sin(\pi/N)]^2C$ is not far less than $del2[m+1]$ and $del2[k+1]$, $del3[n]$ can be used as a saturation detector since $[2\sin(\pi/N)]^3C$ is much smaller than $[2\sin(\pi/N)]^2C$. For example, if C = 200 A and N = 64, then $[2\sin(\pi/N)]^3C$ = 0.188 A. In the interval $n \le m$, the values of $del3[n]$, which is a sinusoid, are equal to or less than 0.188 A.

At $n = m+1$ (saturation start),

$$del3[m+1] = i_{22}[m+1] - 3i_{21}[m] + 3i_{21}[m-1] - i_{21}[m-2] \quad (11)$$

The approximation of (12) can be made with a maximum error of 0.188 A.

$$i_{21}[m+1] - 3i_{21}[m] + 3i_{21}[m-1] - i_{21}[m-2] \approx 0 \quad (12)$$

Thus, $del3[m+1]$ can be approximated as $i_{22}[m+1] - i_{21}[m+1]$, which is nearly the same value as $del2[m+1]$.

At $n = m+2$ (next sample of the saturation start),

$$del3[m+2] = i_{22}[m+2] - 3i_{22}[m+1] + 3i_{22}[m] - i_{21}[m-1] \quad (13)$$

As $i_{22}[m+2] - 3i_{22}[m+1] + 3i_{22}[m] - i_{22}[m+1] \approx 0$ with the maximum error of 0.188 A, $del3[m+2] \approx i_{22}[m-1] - i_{21}[m-1] \neq 0$. In the saturated period, $m+3 \le n \le k$, the magnitude of $del3[n]$, which is also sinusoid, is much smaller than observed before saturation.

At $n = k+1$ (saturation end),

$$del3[k+1] = i_{23}[k+1] - 3i_{22}[k] + 3i_{22}[k-1] - i_{22}[k-2] \quad (14)$$

Since $i_{22}[k+1] - 3i_{22}[k] + 3i_{22}[k-1] - i_{22}[k-2] \approx 0$ with the error bound of 0.188 A, $-del3[k+1] \approx i_{23}[k+1] - i_{22}[k+1]$, which has nearly the same magnitude as $del2[k+1]$.

Similarly, at $n = k+2$ (next sample of the saturation end),

$$\begin{aligned} del3[k+2] &= i_{23}[k+2] - 3i_{23}[k+1] + 3i_{23}[k] - i_{22}[k-1] \\ &\approx i_{23}[k-1] - i_{22}[k-1] \neq 0 \end{aligned} \quad (15)$$

In the period, $k+3 \le n$, $del3[n]$ is also a sinusoid.

Consequently, $del3[m+1]$ and $del3[k+1]$ have nearly the same magnitude as the corresponding values of $del2[n]$ whilst the magnitudes of the sinusoid in $del3[n]$ are reduced more than those of $del2[n]$. Therefore, $del3[n]$ can be used as a saturation detector since $del3[m+1]$ and $del3[k+1]$ are much larger than $[2\sin(\pi/N)]^3C$.

2.4 Criteria for saturation detection

Saturation detection can be based on either $del2[n]$ or $del3[n]$. The choice depends on the values of C and N. Generally, $del3[n]$ when saturation begins or ends is much larger than $[2\sin(\pi/N)]^3C$. Consequently, $del3[n]$ is more effective than $del2[n]$ and is used as the saturation detector in this paper. The detection criteria is based on (16). The samples that satisfy (16) determine the start or end of the saturation period. The saturation and non-saturation is determined by the state of the preceding period.

$$|del3[n]| > Th \quad (16)$$

where Th is a threshold value determined using

$$Th = k\sqrt{2}I_{f\max}[2\sin(\pi/N)]^3 \quad (17)$$

where $I_{f\max}$ is the maximum fault current and k is a margin factor that takes into account the behaviour of the low-pass filter and the sensitivity of the algorithm.

2.5 For a very small time constant during saturation

If the magnetization inductance in a saturated region is very small, the current during saturation rapidly collapses to zero. Thus, the exponential term in $del1[n]$ is less reduced. The exponential terms in $del3[n]$ remain some samples after the saturation start where $del3[n]$ might be larger than the threshold. Therefore, the detector should keep the previous state for those samples even though (16) is satisfied.

The saturation end can also be detected as in the former cases.

2.6 Countermeasure for a spike

Sometimes, A/D conversion may cause a spike signal on the A/D converted current signal. As the third-difference signal has a larger value at the instant, the algorithm may give erroneous results. Thus, in this subsection, the countermeasure for a spike signal is described.

Table 1 shows the secondary current and its differences if the current has a spike, i.e., Δi at $n = s$, which can be positive or negative. As shown in Table 1, $del3[n]$ at $n = s$ has a large value with the magnitude of about Δi. This can cause the algorithm to provide erroneous results. At $n = s+1$, $del1[n]$ may change its sign depending on the situation. On the contrary, $del2[n]$ and $del3[n]$ change their signs. In addition, $del3[n]$ is three times the magnitude of a spike, i.e., $3\Delta i$ because $del3[s+1]$ is negligible compared with $3\Delta i$. Thus, though $del3[n]$ at a instant exceeds a threshold for

saturation detection, the detector does not change its state if $del2[n]$ and $del3[n]$ change their signs and $del3[n]$ has a large value at the next sample. Consequently, the final saturation detection is delayed one sample for discriminating between saturation and a spike. Fig. 2 shows the flowchart of the propose algorithm with the countermeasure for the spike.

Table 1 Current and its differences when a spike exists

sample	s	s+1	s+2
$i_2[n]$	$i_2[s]+\Delta i$	$i_2[s+1]$	$i_2[s+2]$
$del1[n]$	$del1[s]+\Delta i$	$del1[s+1]-\Delta i$	$del1[s+2]$
$del2[n]$	$del2[s]+\Delta i$	$del2[s+1]-2\Delta i$	$del2[s+2]+\Delta i$
$del3[n]$	$del3[s]+\Delta i$	$del3[s+1]-3\Delta i$	$del3[s+2]+3\Delta i$

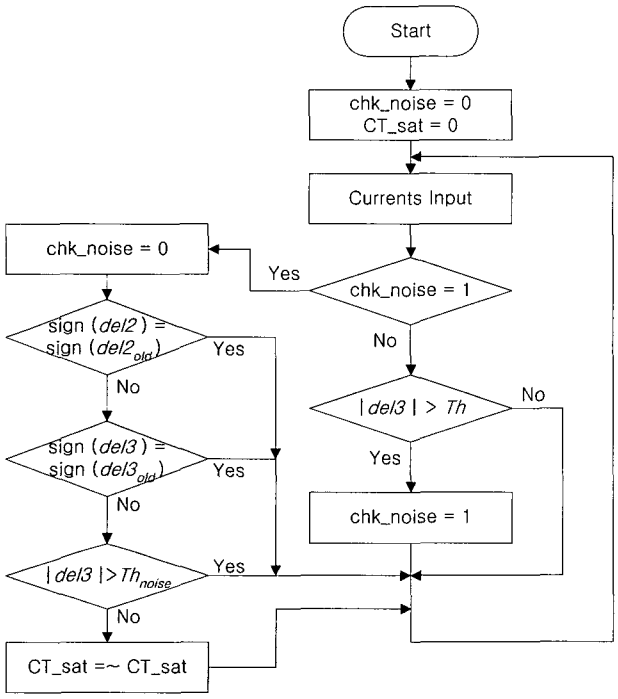

Fig. 2 The flowchart of the proposed detection technique

3. Case Studies

Fig. 3 is a single line diagram of a typical Korean 345 kV transmission line. The simulated fault is an A phase-to-ground fault at a distance 2 km from the P bus. The fault inception angle is zero degrees, i.e., at A-phase voltage minimum. The primary time constant of the source is 20 ms.

The CT modelling method that Kezunovic described [6] is used to simulate the remanent flux in the core. A C400 CT (2000:5) is used for the case studies and connected to a resistive burden of 3.42 Ω. The saturation point of (2.047 A, 1.512 V) is selected to generate hysteresis data using HYSDAT, an auxiliary program in EMTP.

The secondary current contains a point of inflection at fault occurrence. This also may result in a peak in $del3[n]$ that can be detected as the saturation start. To prevent errors in this case, the algorithm is activated only if the current exceeds three times the rated secondary current for three successive samples.

The sampling rate is 64 samples/cycle and all the currents are passed through a low-pass filter with a cut-off frequency of 1920 Hz, which is half the sampling frequency.

The performance of the algorithm was tested on the various magnetization inductances in the saturated region.

Fig. 4 shows the results in the case of a 0% remanent flux. The dotted and solid lines in Fig. 4a are the unsaturated and saturated secondary currents. The distorted secondary current is continuous and has points of inflection at the start and end of each saturation period.

In this case, the discontinuity in $del1[n]$ arises at the next sample after the saturation period has started or ended; $del1[n]$ has a transient value at the sample between the unsaturated and saturated states (see Fig. 4b). This results from asynchronism at the start or end of each saturation period between the sampled current $i_2[n]$ and the original current.

Thus, $del2[n]$ consists of a sinusoid except for the two samples after the saturation start and end. The magnitudes of sinusoids in $del2[n]$ are reduced to about 1.02 A (Fig. 4c). For this example, $del2[n]$ cannot be used as a saturation detector because 1.02 A is only slightly smaller than the values of $del2[n]$ seen at the start or end of each saturation period.

The magnitudes of the sinusoids in $del3[n]$ are reduced to about 0.10 A (Fig. 4d) whereas the values of $del3[n]$ at the start and end of saturation periods are significantly larger. Consequently, $del3[n]$ is used to detect the start and end of each saturation period.

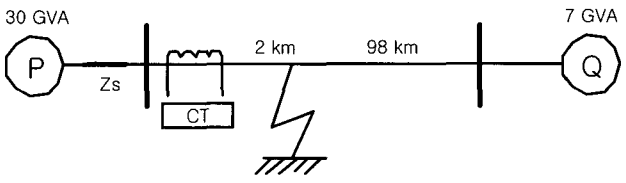

Fig. 3 Simulated power system model

The threshold for secure detection of the start and end of a saturation period can be set much larger than 0.1 A if the smoothing behaviour of the low-pass filter is ignored. The recommended threshold in this paper is 0.3 A (i.e., k = 3) to cope with the effect of the filter. The detector maintains the former state for four samples once (16) is satisfied. This prevents errors due to the effect of asynchronism and the low-pass filter. In Fig. 4e, level 1 and level 0 corre-

spond to the saturated and unsaturated states, respectively. The results clearly show that the algorithm successfully detects saturation with one sample delay.

As mentioned in Section 2.5, if the magnetization inductance in the saturated region is very small, the secondary current rapidly collapses to zero when the CT saturates. The performance of the algorithm is tested when the secondary time constant is very small. Previously, the magnetizing inductance above the knee point was 11.6 mH. The algorithm is now tested when the inductance in the saturated region is reduced first to 50% of 11.6mH (5.8mH) and then to 10% of 11.6 mH (1.16 mH).

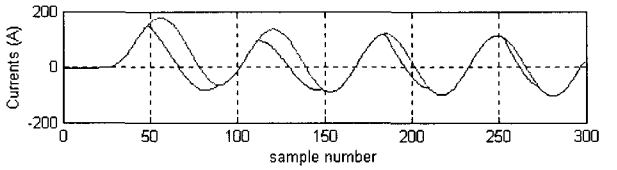

(a) Secondary currents

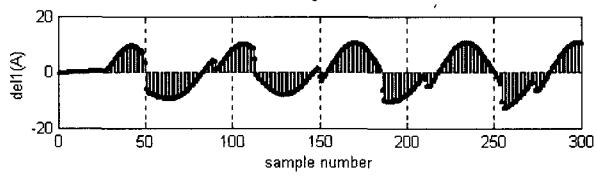

(b) $del1[n]$

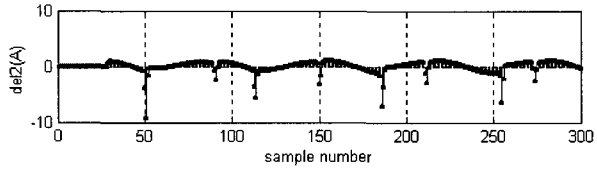

(c) $del2[n]$

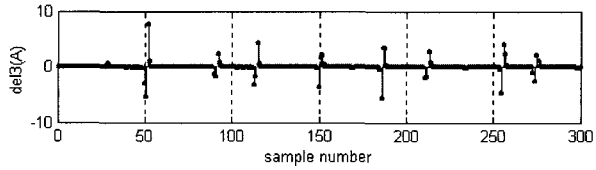

(d) $del3[n]$

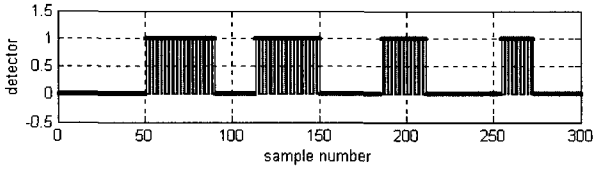

(e) Saturation detector output

Fig. 4 The results in the case of 0% remanent flux

Fig. 5 shows the results with 5.8 mH. As the magnetization inductance is half the former, the current after saturation collapses faster than Fig. 4a; $i_2[n]$ contains points of inflection where each saturation period begins and ends. As expected, $del3[n]$ at the start of each saturation period is larger than observed in Fig. 4c, whereas the values at the end of each saturation period are similar. The number of samples where $del3[n]$ is larger than the threshold value and the detector should maintain its former state is slightly increased compared to Fig. 4d. However, the algorithm detects saturation successfully with one sample delay.

Fig. 6 shows the results with 1.16 mH. The current after saturation decreases faster than observed in Fig. 4a and Fig 5a. As in Fig. 6, $i_2[n]$ contains points of inflection where saturation begins and ends. The values of $del3[n]$ at the start of each saturation period are significantly larger than the equivalent sample values in Fig. 5c, whilst the values at the ends of the saturation period are similar. The number of samples where $del3[n]$ at the start and end of saturation are larger than the threshold value and the detector should keep its former state is increased compared to Fig. 5d.

The results of the above cases indicate that the proposed algorithm detects saturation successfully with one sample delay even if the magnetizing inductance is very low and the current collapses to zero when the CT saturates.

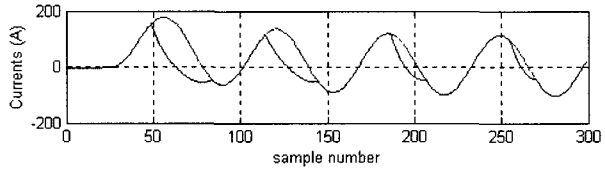

(a) Secondary currents

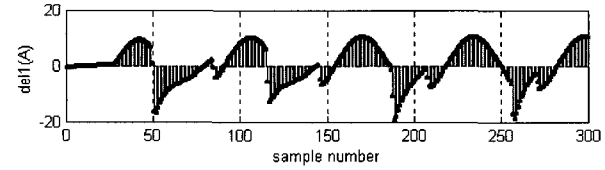

(b) $del1[n]$

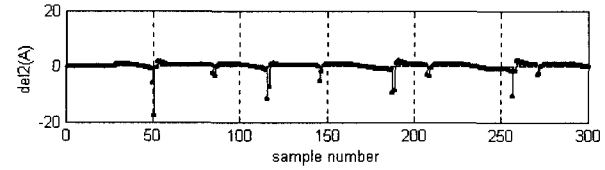

(c) $del2[n]$

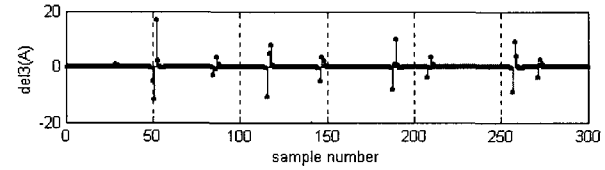

(d) $del3[n]$

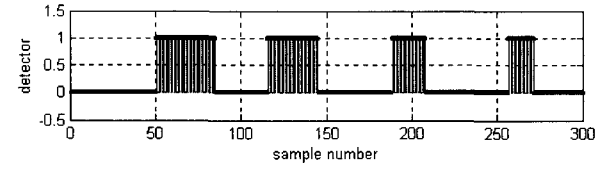

(e) Saturation detector output

Fig. 5 The results in the case of 0% remanent flux with 50% saturated magnetizing inductance value

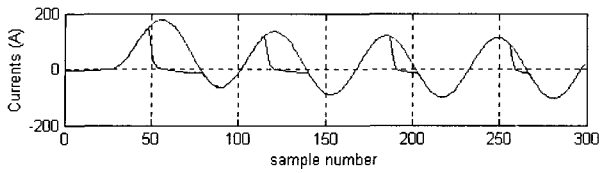

(a) Secondary currents

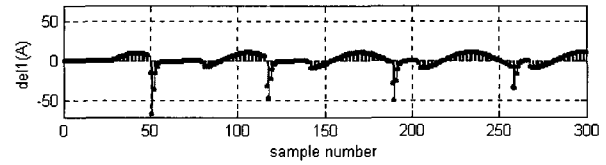

(b) *del*1[*n*]

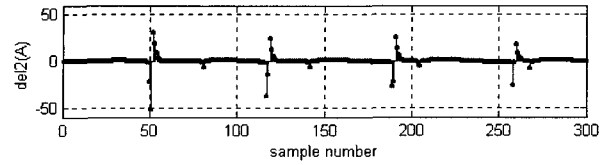

(c) *del*2[*n*]

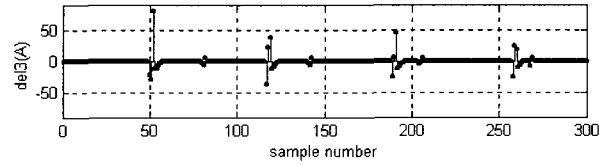

(d) *del*3[*n*]

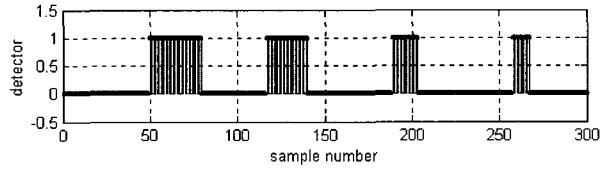

(e) Saturation detector output

Fig. 6 The results in the case of 0% remanent flux with 10% saturated magnetizing inductance value

4. Hardware Implementation

In practice, a real current signal may contain a noise signal resulting from quantization error and so on. Since the proposed algorithm employs *del*3[*n*], it could amplify the noise signal. Therefore, the algorithm is tested under practical conditions, and this section shows the results of hardware implementation of the proposed algorithm into a TMS320C6701 DSP, particularly when spikes occur in the analog-to-digital (A/D) converted signal.

The configuration of the hardware implementation is shown in Fig. 7. Three-phase currents generated by EMTP are converted into analog signals using a PCL-727 digital-to-analog (D/A) board and then injected into the DSP board through the first-order RC filter with a cut-off frequency of 1920 Hz, i.e., half the sampling frequency.

Fig. 8 shows the results in cases of a 0% remanent flux with the magnetization inductance of 11.6 mH. As shown in Fig. 8, *del*3[*n*] is noisier than the simulation results; thus, the threshold value is set to be 1.5 A, which is five times than the simulation cases. The results are very similar to those observed in Fig. 4. The algorithm successfully detects saturation with a larger threshold value than simulation.

Fig. 9 shows the results when spikes, resulting from the A/D conversion, exist in the current. The values are approximately –0.8 A and +0.7 A at n = 253 and n = 277, respectively, which are very small and are not seen clearly in the current in Fig. 9a. *del*3[*n*] has larger values than the threshold at those instants. However, as shown in Fig. 9c and Fig. 9d, at n = 254 and n = 278, which are the next samples of a spike, *del*2[*n*] and *del*3[*n*] change their signs and *del*3[*n*] have large values. Thus, the test results clearly indicate that the proposed countermeasure can discriminate between spikes and the start and end of each saturation period.

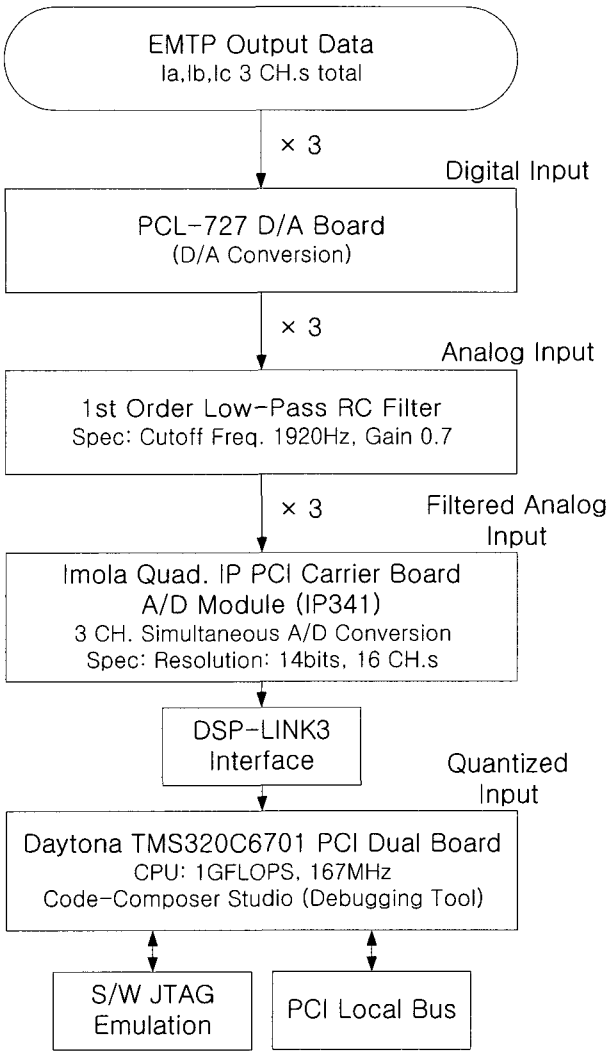

Fig. 7 Configuration of hardware implementation

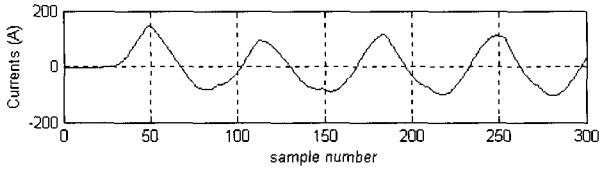

(a) Secondary currents

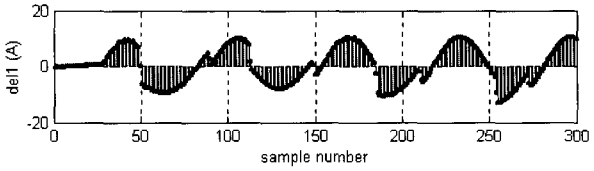

(b) *del*1[*n*]

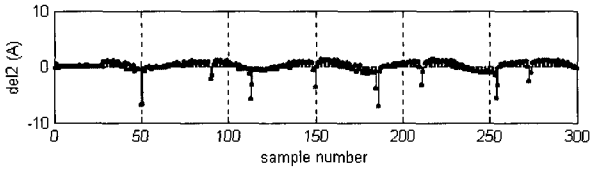

(c) *del*2[*n*]

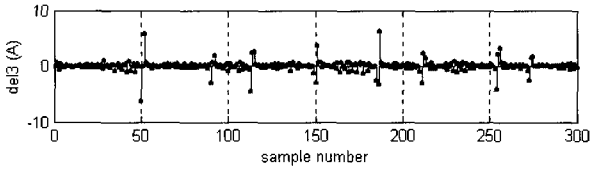

(d) *del*3[*n*]

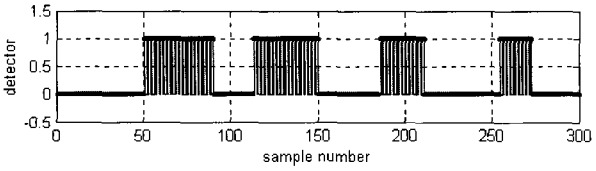

(e) Saturation detector output

Fig. 8 Hardware implementation results for 0% remanent flux

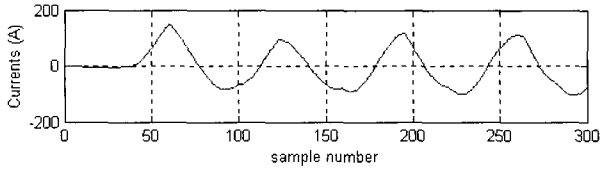

(a) Secondary currents

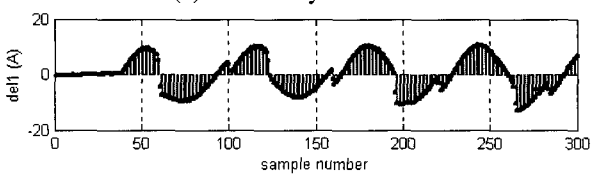

(b) *del*1[*n*]

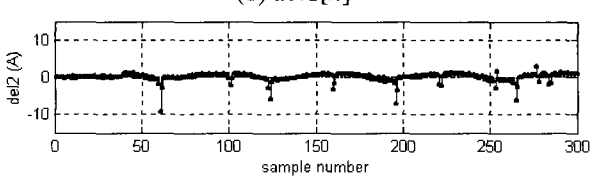

(c) *del*2[*n*]

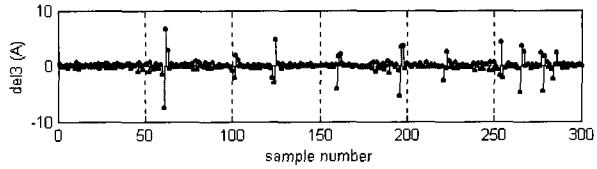

(d) *del*3[*n*]

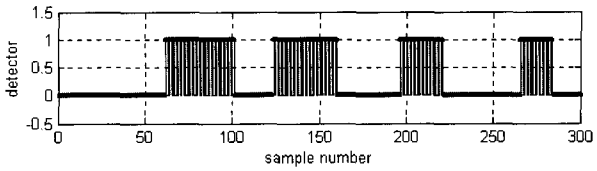

(e) Saturation detector output

Fig. 9 The results when a noise signal exists

5. Conclusion

This paper describes the design of a CT saturation detection algorithm using the third-difference function incorporated with the countermeasure for a spike signal. The magnitude of the third difference function at a point of inflection, which corresponds to the start or end of each saturation period, is much larger than the magnitude seen before, during, or after saturation. This sudden increase in magnitude is used to determine whether the CT is saturated. A prototype monitoring system, based on the described algorithm, successfully detected saturation when it is implemented under practical conditions. The proposed detection method detects the start and end of each saturation period even when a spike signal exists.

Acknowledgements

Authors would like to thank the Korea Ministry of Science and Technology and the Korea Science and Engineering Foundation for their support through the ERC program.

References

[1] A. G. Phadke and J. S. Thorp, *Computer Relaying for Power Systems*, Research Studies Press LTD., 1988, pp. 185–186.

[2] Y. C. Kang, J. K. Park, S. H. Kang, A. T. Johns, and R K. Aggarwal, "An Algorithm for Compensating the Secondary Current of Current Transformers," *IEEE Trans. on PWRD*, Vol. 12, No. 1, January 1997, pp. 116–124.

[3] C. Fernandez, "An Impedance-Based CT Saturation Detection Algorithm for Bus-Bar Differential Protection." *IEEE Trans. on PWRD*. Vol. 16. No. 4. October

2001, pp. 468–472.
[4] Y. C. Kang, S. H. Ok, J. S. Yun, and S. H. Kang, "Performance Analysis of a Lowpass Filter on a CT Saturation Detection Algorithm," *Trans. KIEE A*, Vol. 51, No. 10, October 2002, pp. 495–501.
[5] S. H. Horowitz and A. G. Phadke, *Power System Relaying*, Research Studies Press LTD., 1992, pp. 56–57.
[6] M. Kezunovic, L. Kojovic, A. Abur, C. W. Fromen, and F. Phillips, "Experimental Evaluation of EMTP-Based Current Transformer Models for Protective Relay Transient Study," *IEEE Trans. PWRD*, Vol. 9, No. 1, January 1994, pp. 405–413.

Yong-Cheol Kang
He received the B.S., M.S., and Ph.D. degrees from Seoul National University, Seoul, Korea, in 1991, 1993, and 1997, respectively. He was a visiting scholar at Bath University in 1994. He is now an assistant professor at Chonbuk National University, Chonju, Korea. His research interest is development of new protection schemes for power systems using digital signal processing techniques.

Jae-Sung Yun
He received the B.S. and M.S. degrees from Chonbuk National University, Chonju, Korea in 1997 and 1999, respectively. He is now studying for his Ph.D. degree at Chonbuk National University. His research interest is power system protection.